Film thicknesses influence on the interfacial thermal resistances within Ge-Rich Ge_2 Sb_2Te_5 /Ge_2Sb_2Te_5 multilayers

Clément Chassain, Andrzej Kusiak, Cécile Gaborieau, Yannick Anguy, Nguyet-Phuong Tran, Chiara Sabbione, Marie-Claire Cyrille, Jean-Luc Battaglia

Film thicknesses influence on the interfacial thermal resistances within Ge-rich $Ge_2Sb_2Te_5/Ge_2Sb_2Te_5$ multi-layers

Clément Chassain[1],* Andrzej Kusiak[1], Cécile Gaborieau[1], Yannick Anguy[1], Nguyet-Phuong Tran[2], Chiara Sabbione[2], Marie-Claire Cyrille[2], and Jean-Luc Battaglia[1]
[1] *I2M Laboratory Bordeaux University,* [2] *CEA LETI*

Phase change memories (PCRAM) are often made of chalcogenide alloys in the form of multilayer systems (MLS). One of the most used alloys are $Ge_2Sb_2Te_5$ and Ge-rich $Ge_2Sb_2Te_5$. This article reports on the thermal characterization of very thin (<5 nm) Ge-rich $Ge_2Sb_2Te_5$ /$Ge_2Sb_2Te_5$ MLS. by Modulated Photothermal Radiometry (MPTR). The MPTR method allows for the investigation of such samples by determining, with an inverse method, the total thermal resistance of the stack deposited on the substrate. With the measurement of the total thermal resistance it is possible to determine the thermal conductivity of the deposit and the interfacial thermal resistances between layers. The interfacial thermal resistance between Ge-rich $Ge_2Sb_2Te_5$ /$Ge_2Sb_2Te_5$ was characterized, which is an important parameter to reduce the energy cost of the PCRAM functioning. It was also possible to highlight a decrease in interfaces quality inside the MLS after the beginning of the phase transition around 250°C.

I. INTRODUCTION

In the field of non volatile memories, phase change materials (PCM) are widely studied for their use in the phase-change RAM or PCRAM [1–4]. The chalcogenide alloys involved in those devices are made at least from one chalcogenide element such as . Se, Te, S. The most characterized associations of chalcogenide elements are based on In-Sb-Te and Ge-Sb-Te systems. The electrical resistivity R_e of these alloys varies along decades depending on their crystalline state, which make them great candidates for non-volatile memory devices. In the amorphous state, the electrical resistivity is high and the material behaves as an insulator whereas, in the crystalline state, the electrical resistivity is significantly lower. This change of properties allows to link a bit 1 or 0 or even intermediate [4, 5] to the electrical state. It is also important to measure the thermal properties of PCM for their use in PCRAM [6–8]. Knowing precisely the thermal properties as a function of the temperature and depending on the crystalline state is mandatory to determine the electrical power required for the phase change. The SET programming of the PCRAM is responsible for the transition from the insulating state to the conductive state whereas the RESET programming of the PCRAM is responsible for the reverse change. The PCRAM devices have been scaled down for the past few years to the point of reaching the nanometer scale [6, 7]. As the transitions duration for the phase change and the energy consumption are reduced with the technological improvements, the alloy implementation went from the so-called "mushroom" programming volume [9, 10] to nanowires [11–13] with a few nanometers diameter or even PCM supperlattices leading to the inter-facial phase change memory technology [14]. Moreover, other PCRAM configurations have been explored by industrials, notably by Samsung, IBM, Intel/Micron (XPoint) and Hynix/Ovonyx [15–17]. The low scale of the PCRAM makes necessary to control the cross-talks effects with neighboring cells [18, 19]. It is shown that the thermal boundary resistance (TBR) between PCM micro volume and neighboring materials such as the metal electrodes and the dielectrics has an influence of the same order as the thermal conductivity for the heat transfer within the device [18, 20–22]. The measurement of the thermal resistance or conductance of these nanostructured materials can hardly be achieved due to their low scale.

The most common chalcogenide alloy in the framework of PCRAM is $Ge_2Sb_2Te_5$ (GST) mainly due to its fast transformation rate and high cyclability [9]. In today's PCRAM applications one of the most limiting parameter of GST is its low crystallization temperature (150°C) guaranteeing data retention up to 10 years at 75°C only. Thus it is not appropriate for applications where operations at temperatures higher than the crystallization temperature of the GST are realized. This limitation motivates new research works in order to engineer new materials to improve the PCRAM performance. The two main focus points are the improvement of the stability of the amorphous phase to increase data retention performances, and the reduction of current needed for the RESET operation. Indeed, by reducing the current, the programming energy is reduced and therefore the cross-talks risks lowered. One of the way to tune the GST properties is by doping it with carbon [23, 24], nitrogen [25, 26], silicon [27, 28] and/or Ge atoms (GeGST) [29, 30]. The GeGST or Ge-rich GST has a higher crystallization temperature than GST which ensures a better thermal stability of the reset state. Another benefit of the Ge-rich GST is its higher electrical resistivity compared to the GST [31] which means that the current needed for the Joule effect during the reset cycle is lower for the GeGST compared to the current needed for the GST. However, studies show that after annealing at high temperature (>450°C) multiple phase segregation took place. Indeed,

* clement.chassain@u-bordeaux.fr

Sb, Ge and Te atoms are scattered through PCM in an inhomogeneous way [32, 33]. This undesirable phenomenon is not reported as completely detrimental. In fact, the memory cell after a stable segregation show an improvement in endurance [34], which illustrates the interest for the use of the Ge-rich GST. In order to extend the advantages of the tuned PCM, multi-layers composed of them started to be implemented in memory cells [20, 35–37]. Having multiple layers of PCM will slow down heat diffusion since the phonons will face obstacles at the interfaces, thus reducing the cost of heating the PCM and also improving heat confinement. Using multi-layers PCM also allows for an increase of temperature crystallization. PCM layers are indeed under greater stress while heating, leading to a higher activation energy and more linear grain shapes. The difference in electrical resistivity between GeGST, GST and GeGST(10nm)/GST(10nm) multi-layers is measured in the literature [31] and shows that the resistivity contrast between the amorphous and crystalline phase is usually much larger for the multilayer structure than for the mono-layer structure. However, using multi-layer PCRAM means that interfacial thermal resistances between layers need to be well characterized. It is important to determine the value of the said resistances but also to study their dynamics while heating. A decrease in the interfaces quality while heating can have detrimental effects on the functioning.

In this work we implement the Modulated Photothermal Radiometry (MPTR) configuration within the infrared domain (IR) for thermal characterization of GeGST/GST multilayer systems (MLS). This method has been fully detailed in the literature [38] and several applications to PCM have been reported [39, 40]. In the present work, interfacial thermal resistances between GeGST and GST values are given for the amorphous phase. It is also shown that the quality of the interfaces starts to decrease as soon as the crystallization happens. Such characterization requires experimental work since simulating interfaces integrity over the phase transition can be very complex. However, concerning the value of the interfacial thermal resistance between GeGST and GST in the amorphous state, the experimental work realized in this paper is in good concordance with some theoretical models.

II. EXPERIMENTAL CONDITIONS

A. Experimental setup

The schematic view of the setup is presented in Fig. 1 and is explained in details in reference [41]. The temperature of the sample is driven by commercially available oven working under argon as inert gas. Samples are characterized from room temperature to 400°C, then cooled again to room temperature. The thermal perturbation seen by the sample is generated by a laser of 1064 nm wavelength and 1.7 W maximum power. The laser spot radius is 0.8 mm. An acousto-optic modulator enables the modulation of the laser using the squared signal coming from a function generator. The thermal response is then measured by an infrared HgCdTe detector with an infrared sensitive element of 0.5 mm in diameter. A lock-in amplifier was used to measure the amplitude and the phase lag ϕ between the reference and the detector output according to the frequency f. The reference signal used for the lock-in detector is the TTL signal issued from the function generator. In order to avoid the phase lag induced by the modulator and the measurement chain, a calibration was realized on an already well characterized bulk semi-infinite sample. The calibration function is found as: $\phi_{real} = \phi_{exp} + 7.49e^{-4}f - 0.14$ for frequencies ranging from 100 Hz to 10 kHz. In addition, the real temperature of the sample at a given controlled temperature of the furnace has been calibrated using an infrared camera. The temperature T of the sample according to that of the furnace is found as: $T = 0.8685T_{oven} + 12.24$.

B. Sample preparation

The GeGST/GST MLS have been fabricated by magnetron sputtering, using a mixture of argon and nitrogen as sputtering gas. The samples are made in 4 variations with different unit layer thickness (e_{GeGST} and e_{GST}) repeated N times but resulting in the same total film thickness: $e_{MLS} = (e_{GeGST} + e_{GST})\,N \approx 100\,\text{nm}$. The stacks compositions are reported in Table I. The configuration for MPTR setup is presented in Fig. 2. The GeGST composition is obtained using co-sputtering from two stoichiometric targets, namely, Ge and $Ge_2Sb_2Te_5$. The Ge-rich composition used is referred as "GST + Ge 45%" where 45% is the nominal fraction of the Germanium added to the $Ge_2Sb_2Te_5$ reference alloy [29]. The GeGST/GST layers have been deposited onto 200 mm in diameter silicon wafers (750 μm in thickness) covered by a 300 nm thick Si_3N_4 (SiN) passivation layer. The sputtering gas used (mixture of Ar and N_2) was chosen to ensure a nominal N doping of 7% of the GeGST film. Nitrogen addition inside the layer is proven to enable a finer grain structure in the films and also to increase the crystallization temperature [42–45]. The GeGST/GST MLS are deposited in the amorphous phase for both constituents. Transmission electron microscopy (TEM) and Energy-dispersive X-ray spectroscopy (EDX) images have been realized on the different configurations to control the quality of the interfaces after deposition. The TEM and TEM EDS analysis for a (GST 1.5nm/GST+Ge45% 1.5nm)x15 configuration are provided in Fig. 3. It is shown that interfaces inside the MLS are well defined before annealing. Following the deposition of the GeGST/GST multi-layers, all samples were covered by sputtering with a 100 nm thick platinum film in order to obtain a optical to thermal transducer for photothermal measurements and to avoid possible oxidation and evaporation of the MLS at high temperature. A

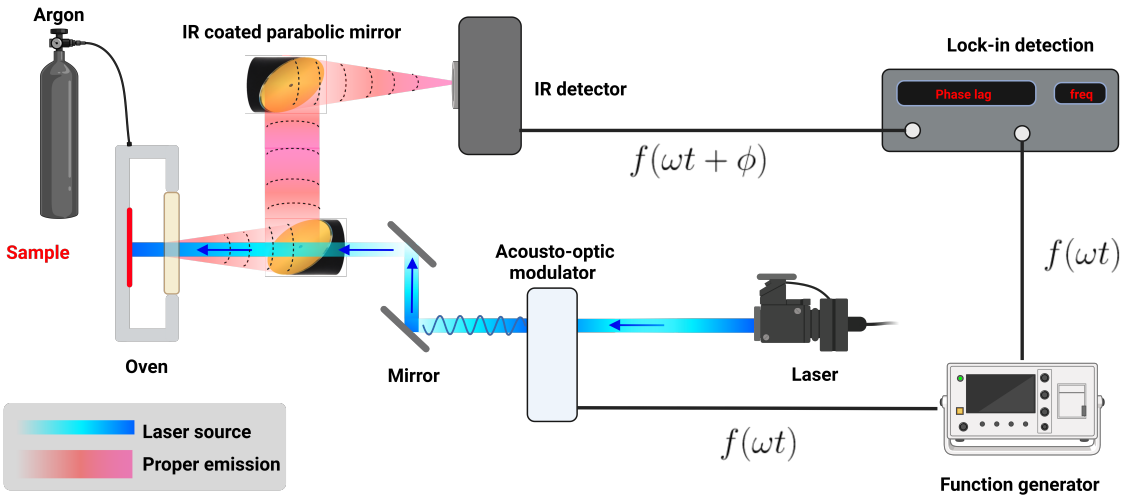

Figure 1: Schematic description of the MPTR experimental setup. The sample is put inside a furnace that permits reaching up to 1200°C under an inert gas.

10 nm thick TiN layer is deposited on the MLS to improve the Pt adhesion.

III. MATHEMATICAL DETAILS AND MODELING

The periodic temperature variation $\Delta T(\omega)$ at the surface of the sample being small enough, it is assumed that the measured proper emission seen by the IR detector is linearly proportional to $\Delta T(\omega)$. Under the assumption of 1D heat transfer within the sample, with no heat loss and a semi-infinite medium behavior for the substrate, it is established a simple relationship between the temperature change $\Delta T(\omega)$ and the heat flux $\varphi_0(\omega)$ at a given pulsation $\omega = 2\pi f$ (f is the frequency) as [46, 47]:

$$\frac{\Delta T(\omega)}{\varphi_0(\omega)} = Z_{Si}(\omega) + RTH \tag{1}$$

where $Z_{Si}(\omega) = 1/\left(E_{Si}\sqrt{j\omega}\right)$, with $E_{Si} = \sqrt{(\rho Cp)_{Si} k_{Si}}$ (ρ is the density, Cp is the specific heat and $k_{Si}$is the thermal conductivity of the silicon wafer and $j^2 = -1$), is the thermal impedance of the wafer, and RTH is the thermal resistance of the (Pt/TiN/MLS/SiN) stack. The thermal conductivity of the silicon wafer is reported in Table II and $(\rho Cp)_{Si} = -2.64T^2 + 2.11e^3 T + 1.57e^6$ J/m^3/K. The phase lag $\phi(\omega)$ is calculated from (1) as :

$$\phi(\omega) = \tan^{-1}\left(\frac{-\sqrt{\frac{a_{Si}}{2\omega k_{Si}^2}}}{\sqrt{\frac{a_{Si}}{2\omega k_{Si}^2}} + RTH}\right) \tag{2}$$

where $\alpha_{Si} = k_{si}/(\rho C_p)_{Si}$ is the thermal diffusivity. The Levenberg-Mardquardt [48–50] minimization algorithm is used to minimize the gap between the experimental data and the model, allowing the identification of the total thermal resistance of the stack RTH. Assuming the Pt and TiN layers fully thermalized at each pulsation ω, the thermal resistance RTH of the stack is expressed as:

$$RTH = N\left(\frac{e_{GeGST}}{k_{GeGST}} + \frac{e_{GST}}{k_{GST}}\right) + (2N-1)TBR_{GeGST/GST} + \frac{e_{SiN}}{k_{SiN}} + TCR \tag{3}$$

With:

$$TCR = TBR_{Pt/TiN} + TBR_{TiN/GeGST} + TBR_{SiN/Si} + TBR_{GST/SiN} \tag{4}$$

where e_i and k_i denote respectively the thickness and the thermal conductivity of layer i, N is the number of repe-

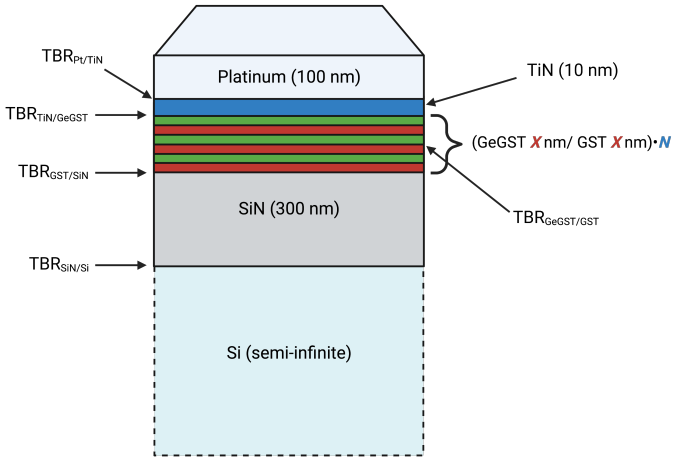

Figure 2: Schematic view of the sample composition. The GeGST/GST MLS configurations are reported in Table I. A Pt film is deposited to act as an optical to thermal transducer. The TiN layer improves the adhesion of Pt. The stack involves several interfacial thermal resistances. The sum of those thermal boundary resistances is depicted as $TCR = TBR_{Pt/TiN} + TBR_{TiN/GeGST} + TBR_{GST/SiN} + TBR_{SiN/Si}$. X denotes the thicknesses of the PCM layers and N denotes the number of times the GeGST/GST unit cell is repeated to make the stack.

Sample label	Deposit constitution	Deposit thickness
P05	(GST 10nm/GST+Ge45% 10nm)x5	100 nm
P10	(GST 5nm/GST+Ge45% 5nm)x10	100 nm
P17	(GST 3nm/GST+Ge45% 3nm)x17	102 nm
P33	(GST 1.5nm/GST+Ge45% 1.5nm)x33	99 nm

Table I: The four GeGST/GST MLS configurations with unit layer thickness of 10, 5, 3, 1.5 nm. The total thickness for the four configurations is 100 nm

	k(T(°C)) (W/m/K)	ref.
SiN	$4.66e^{-9}T^3 - 5.80e^{-6}T^2 + 2.84e^{-3}T + 1.15$	[51]
Si	$5.23e^{-4}T^2 - 0.451T + 144.3$	[Unpublished]
GeGST	0.29	[31]
GST	0.18	[31]

Table II: Parameters required for the calculation of RTH in the amorphous phase from relation (3). References are also indicated for each parameter.

titions of GeGST/GST unit cell in the MLS and $TBR_{i/j}$ denotes the thermal boundary resistance between contiguous layers i and j. The required parameters for the calculation of RTH from relation (3) are reported in Table II.

It is possible to compute a theoretical value of the interfacial thermal resistance between layers using the diffuse mismatch model (DMM) [52]. The expression of the TBR between materials 1 and 2 from the DMM is:

$$TBR_{1\to2} = \left(\sum_j \frac{k_B^4\, T^3}{8\,\pi^2\,\hbar^3\, V_{j,1}^2} \alpha_{1\to2} \int_0^{\Theta_{D,1}/T} \frac{x^4\, e^x}{\left(e^x - 1\right)^2} \mathrm{d}x \right)^{-1}, \quad j = (L,T,T) \tag{5}$$

In this equation, $\hbar$ is the reduced Planck constant, k_B is the Boltzmann constant and V_j is the velocity of the phonons in the different directions (j=(L,T,T), L is the longitudinal direction and T are the two transversal ones). The phonon transmission coefficient α is defined as:

$$\alpha_{1\to2} = \frac{v_{L,2}^{-2} + 2v_{T,2}^{-2}}{v_{L,1}^{-2} + 2v_{T,1}^{-2} + v_{L,2}^{-2} + 2v_{T,2}^{-2}} \tag{6}$$

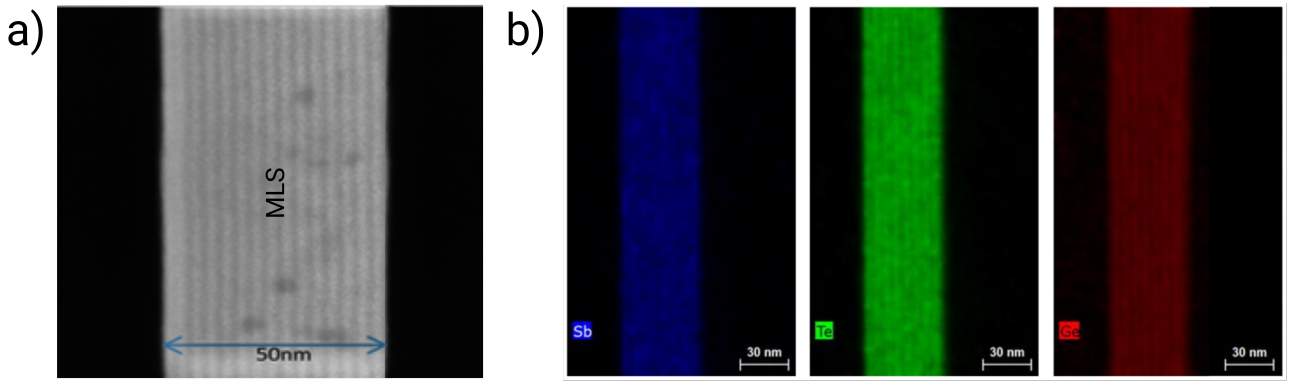

Figure 3: a) Transmission electron microscopy (TEM) image of a (GST 1.5nm/GST+Ge45% 1.5nm)x15 stack configuration sample. b) TEM EDS analysis of a (GST 1.5nm/GST+Ge45% 1.5nm)x15 stack configuration sample.

IV. RESULTS AND DISCUSSION

A. Stack thermal resistance RTH

The samples, listed in Table I, were heated from 50°C up to 400°C with a heating rate of 100°C/min with a short 30 seconds plateau to stabilize the temperature before each acquisition. Each temperature measurement was realized at two frequencies, 2551 Hz and 3182 Hz, which led to a measurement time of 5 minutes per temperature. Those two frequencies were chosen to have a heat penetration depth greater than the stack thickness and to still have the wafer acting as a semi infinite medium. The RTH value is identified after substracting the SiN contribution. Results are reported in Fig. 4 according to the annealing temperature. Previous results for 100 nm thick GeGST [31] and GST [41] are also reported in Fig. 4. Two RTH transitions are observed in Fig. 4. The first one, around 150°C, is rather sharp and is assigned to the well known amorphous to fcc crystalline transition within the GST layers of the MLS. A second smoother and less marked RTH drop is observed around 300°C. The latter is related to the delayed amorphous (am) to fcc crystalline transition within the GeGST layers of the MLS. In between those two RTH drops, the RTH decreases smoothly as T increases. This behavior may be tentatively related to the ongoing diffusion of atomic Ge, which lessens/spreads over T the expected T-lag of the am-to-fcc transition within Ge-doped layers and hinders the fcc-to-hcp transition in the GST layers of the MLS. The results demonstrate also that, in the amorphous phase, increasing the number of interfaces in the MLS, while keeping its thickness constant, leads to increase RTH (at the low temperature range). It is a consistent observation that adding more interfaces leads to increase the total thermal resistance. It is also possible to note a delay (denoted η) in the first transition temperature with the increase of the number of interfaces. However after the first phase transition (above at 250°C), a similar value of RTH it is obtained for each

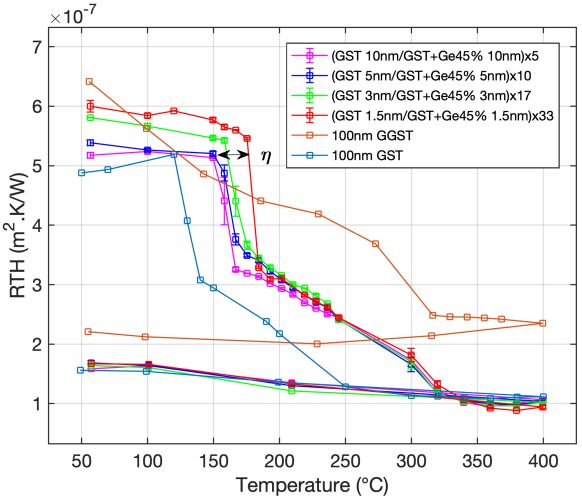

Figure 4: Total thermal resistance of the stack deposited on the silicon wafer for samples P05, P10, P17, P33 and two reference samples. The heating rate is 100°C/min, each temperature measurement required 5 minutes. The sample were in the amorphous phase before heating. After cooling, the samples are in a stable crystalline phase. The SiN contribution to the total thermal resistance RTH was subtracted for MLS and GGST. Regarding the GST, the contribution of the SiO_2 was also subtracted. The difference between $RTH_{GGST}$and thermal resistances from the MLS RTH_{MLS} for the crystalline phase is denoted as ΔRTH. The shift in crystallization temperature from amorphous to fcc is denoted η.

MLS. Moreover, the values of RTH for the MLS are the same as the 100 nm thick GST. This phenomenon can be explained by the loss of interface integrity from both the crystallization process and species inter-diffusion at high temperature. The degradation of interface quality subsequent to heating has been shown already in the literature [53].

B. Interfaces integrity

In-situ Raman scattering analysis from room temperature to 450°C was performed using an INVIA Renishaw confocal spectrometer coupled to a Leica optical microscope. A 785 nm monochromatic laser excitation was used. The temperature of the samples was controlled the same way as the MPTR experiment. The Raman analysis was also conducted under inert argon atmosphere with a 100°C/min heating rate with a short 30 seconds plateau to stabilize the temperature before each spectral acquisition. A low level laser power density was used in order to avoid unwanted additional heating by the incident radiation. The spectrometer is fitted with an edge filter cutting the black-scattered light at ∼100 cm^{-1}. The spectral resolution of the Stokes-side Raman spectra was ∼1 cm^{-1}. The results for the (GST 5nm/GST+Ge45% 5nm)x5 stack are reported in Fig. 5. SEM micrographs of this particular stack after annealing at 410°C were also realized and reported in Fig. 6. At room temperature the main feature of the Raman spectra of the amorphous stack is a large band spreading over the 100-190 cm^{-1} spectral region. This large band, mainly composed of two overlapping bands peaking around 125 $cm^{-1}$and 150 cm^{-1} is comparable to the expected Raman signature of the amorphous as-deposited $Ge_2Sb_2Te_5$ (GST) alloy. At higher frequencies, the $\nu_3(F2)$ antisymmetric stretching mode of tetrahedra in amorphous GeTe, peaking at 220 cm^{-1}, most likely contributed to the broad bulge in the 190 – 300 cm^{-1} region associated with a-Ge in tetrahedral sites within the *N*-doped GeGST sublayers of the MLS [54, 55]. The Raman spectra remained essentially unchanged from room temperature to 130°C. Upon reaching 160°C, the relative intensity of the band at ∼150 cm^{-1}decreased markedly, and shifted towards higher frequencies at around 160 cm^{-1}. The band at ∼125 cm^{-1} shifted towards lower frequencies at about 115-120 cm^{-1}. This evolution can be explained by the transition from amorphous to metastable *fcc* crystalline state within the GST sublayers of the MLS. Regarding the significant drop of the band originally peaking at 150 cm^{-1}, building on the work found in the literature [56], we may argue that the decreasing of this band could be associated with the appearance of a transient GeTe phase within the GeGST. However, it is important to acknowledge that this transient phase would usually appear above 300°C. At 330°C, the Raman spectrum does not evolve significantly with respect to 160°C . At this high temperature, the lowered intensity of the band assigned to Sb-Te vibrations can be explained by the appearance of the aforementioned transient GeTe phase nucleating in the GeGST sublayers [56]. On the other hand, at such a high temperature, one would expect that the GST sublayers that switched to the *fcc* state at lower temperature (160°C) now undergo the transition towards the hexagonal-closed-packed (*hcp*) lattice. Yet, the *fcc*-to-*hcp* transition was essentially not observed. In Fig. 5 (330°C), we merely see two discrete shoulders at 110 and 170 cm^{-1}, which may barely suggest this transition to *hcp*. For reference, the inset in Fig. 5 provides the non ambiguous Raman signature of the GST *hcp* crystalline lattice, much more sharply than the discrete observed shoulders at 330°C. In the current case study, we observe instead a more pronounced signature of the *fcc* transformation, reflected by the increasing relative intensity of the band peaking at about 160 cm^{-1} . This behavior may reflect the onset of the thermally delayed *fcc* transformation within the GeGST amorphous sublayers. According to the literature [56], the delayed thermal crystallization of cubic GST from amorphous GeGST precursors is a three-fold process whereby a transient GeTe phase first appears, which triggers the nucleation and the growth of cubic Ge , cubic GST forming last. Unfortunately, the low signal-to-noise ratio of the Raman spectrum acquired at 330°C did not allow to confirm the presence of cubic Ge around 300 cm^{-1}. At 450°C, the crystallization of *fcc* GST from the GeGST sublayers of the MLS is clearly confirmed by the two broad bands peaking at about 120 cm^{-1} and 160 cm^{-1} . At this high temperature, cubic GST and cubic Ge do coexist [29, 56–58]. The absence of the cubic-to-hexagonal transition at high temperature in GeGST thin films has been reported in the the literature [57]. Thus, an excess of a-Ge with respect to the 225 stoichiometry of GST would prevent the latter transition. As the *hcp* crystal system is here not observed, despite the presence of GST sublayers, we speculated that atomic Ge may migrate from GeGST sublayers into GST sublayers after the amorphous to *fcc* transition around 160°C in the latter sublayers. However, the thermal resistance of the MLS being the same as the GST mono-layer one could be a sign of a *fcc* to *hcp* transition happening during cooling. The *fcc* phase being highly metastable and the oven following temperature set-points during cooling, such transition could have happened. The scanning electron micrograph (SEM) of the MLS annealed at high temperature reported in Fig. 6 seem to state only partial mixing. Indeed, some interfaces may be damaged into interphases in the annealed samples, but the sample is still closer to a multi-layered system than a mono-layered system. This may support the partial mixing (diffusion of atomic Ge) between GST and GeGST sublayers.

The in-situ Raman scattering analysis suggests that the germanium migrated in whole the MLS. This migration explains the similitude on the RTH values for MLS and the 100 nm thick GST stack. The phase change allowed the atomic structure of the GeGST/GST multilayers to relax itself and reach its minimum of potential energy by distributing the germanium atoms in all the MLS. Thus, hindering the effect of the doping. It is then possible to consider the crystallization dynamics of the GeGST/GST MLS similar to a pure GST stack even though the GST has been doped with Ge atoms. The difference in thermal resistances ΔRTH illustrated in Fig. 4 is a testimony of the doping being hindered and the MLS being similar to pure GST. Since at high temperatures TCR will most likely decrease, the

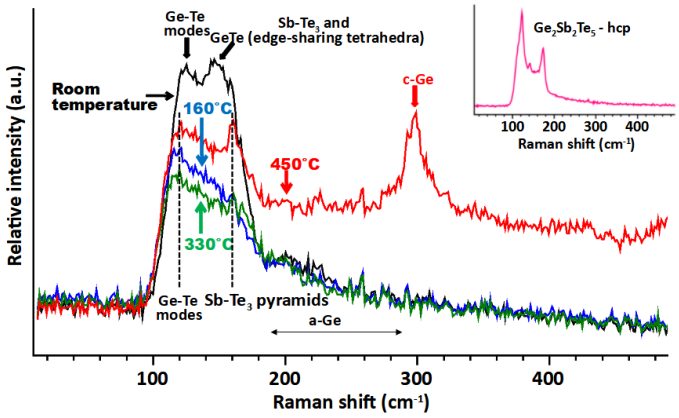

Figure 5: In-situ Raman analysis of a the (GST 5nm/GST+Ge45% 5nm)x5 stack sample. The room temperature spectrum (black), the 160°C spectrum (blue spectrum), the 330°C spectrum (green spectrum) and the 450°C spectrum (red spectrum) are reported on the figure along with a $Ge_2Sb_2Te_5$ *hcp* reference spectrum.

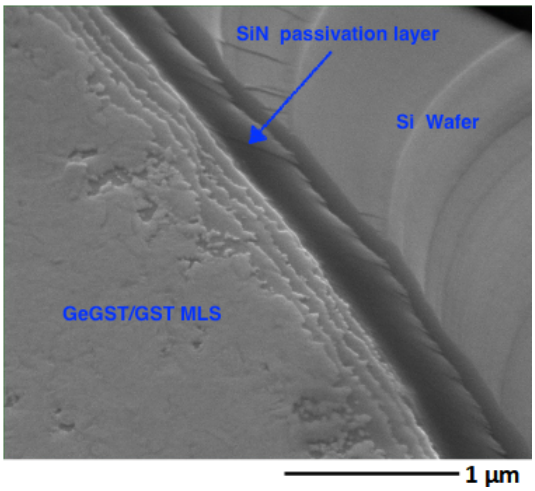

Figure 6: Scanning electron micrograph (SEM) of the (GST 5nm/GST+Ge45% 5nm)x5 stack sample annealed at 410°C. We can see the trace of 5 interphases while the original as-deposited MLS included a vertical alternation of 10 elementary sublayers. This may suggest only a partial mixing between the GST and the GGST sublayers, the interfaces are closer to interphases.

gap ΔRTH can be explained mostly by the change in thermal conductivity between GGST and GST, that is $\Delta RTH \approx e_{MLS}(1/k_{GGST} - 1/k_{GST}) + \epsilon$. The residues ϵ can be for the most part attributed to TCR between samples being slightly different or to small regions of the MLS where interphases are still closer to being interfaces coupled to doping residues.. The thermal conductivities of GGST and GST are reported in Fig. 7. A TiN adhesion layer is present between the Pt layer and the GGST layer for the samples characterized in this

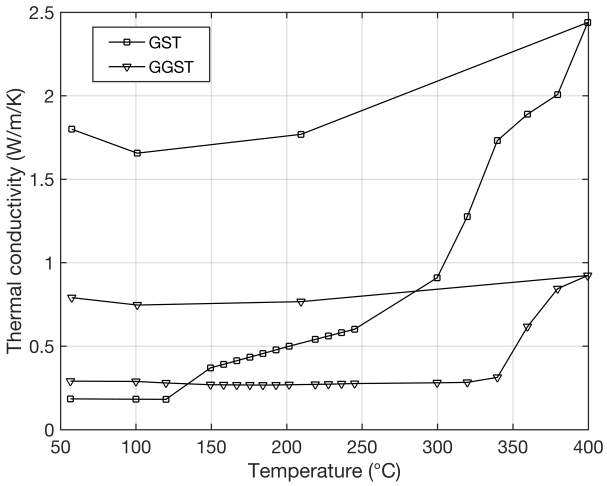

Figure 7: Thermal conductivities of GGST and GST [31].

study. The pure GGST sample was characterized with the Pt directly deposited on the GGST, thus the Pt adhesion is much worse than in the MLS. It means that $TBR_{PT/GGST} > TBR_{Pt/TiN} + TBR_{TiN/GGST}$. This relation has already been confirmed for the amorphous phase by previous work [31, 59] carry on for the crystalline phase. After annealing the MLS is now comparable to a GST stack in terms of thermal properties and $TBR_{GGST/GST}$ tends to 0.

C. Thermal interface resistances characterization

Basing on equation (3), one has:

$$RT = (2N-1)TBR_{GeGST/GST} + TCR \qquad (7)$$

with: $RT = RTH - N\left(e_{GeGST}/k_{GeGST} + e_{GST}/k_{GST}\right) - e_{SiN}/k_{SiN}$. By performing a linear regression on $RT = f(2N-1)$, it is possible to extract the value of $TBR_{GeGST/GST}$ and TCR at the different annealing temperatures. The linear regressions are reported Fig. 8. The results are shown is Fig. 9 considering the temperature range where the MLS is still in its amorphous state. Indeed, as showed in the previous section, the MLS interfaces are damaged at elevated temperature, which does not allow the calculation of a thermal resistance between GeGST and GST layers within the MLS. The average values are $TBR_{GeGST/GST} = (1.39 \pm 0.16).10^{-9}$ m^{2}K/W and $TCR = (1.72 \pm 0.06).10^{-7}$ m^{2}K/W in the amorphous state. As reported in the figure, these values are close to the theoretical values computed by the Diffuse Mismatch Model (DMM), that is $1.23.10^{-9}$m^{2}K/W for $TBR_{GeGST/GST}$, [52] and values found in the literature [31].

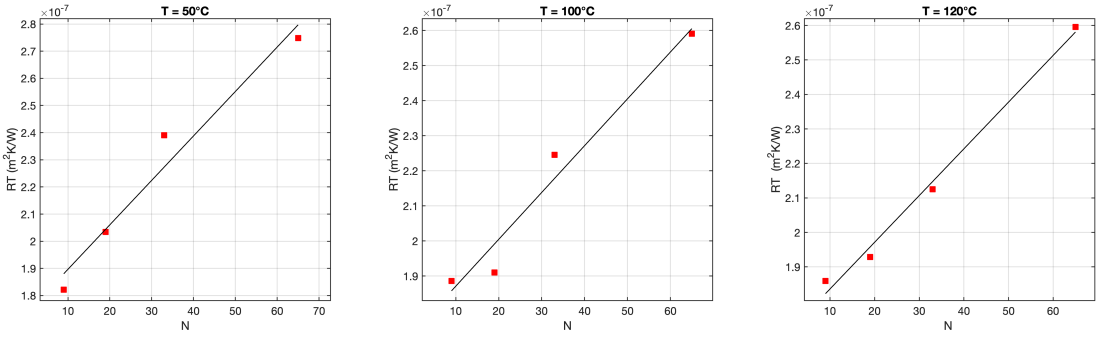

Figure 8: Linear regression for the amorphous phase based on equation (7).

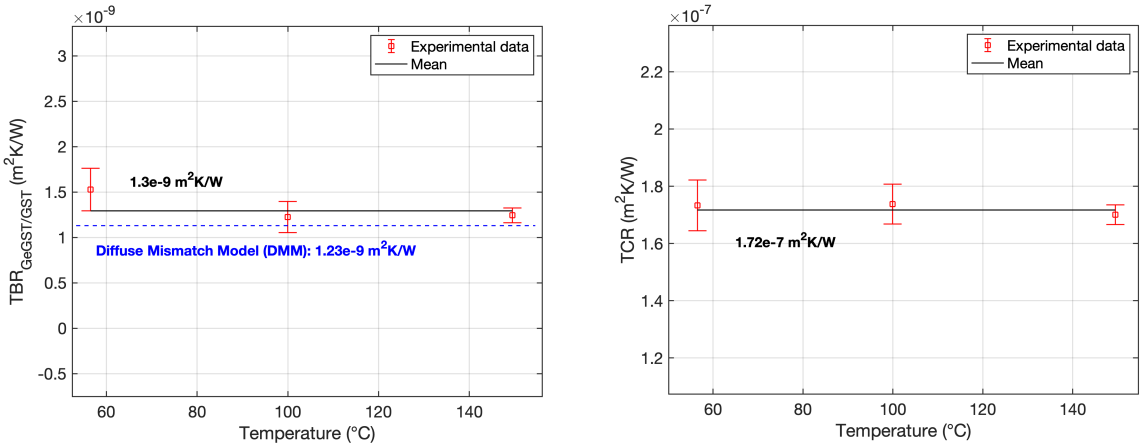

(a) (b)

Figure 9: a) Interface thermal resistance $TBR_{GeGST/GST}$ between a GeGST and a GST layer within the MLS at 3 different temperatures where the MLS is in its amorphous state. The value is compared to theoretical value computed with the DMM. The parameters values used for the DMM computation are reported in Table III. b) Sum of the thermal interface resistances TCR clarified in equation (4) for 3 different temperatures. All the values have been computed by linear regression on equation (7) using the data displayed in Fig. 4.

Layer	Longitudinal speed (m/s)	Transversal speed (m/s)	ref.
GeGST	3600	2530	[60]
GST	2350	1350	[61]

Table III: Phonon velocities used for the theoretical computation of $TBR_{GeGST/GST}$ using the DMM.

V. CONCLUSION

In this work it was shown that increasing the number of interfaces in the phase change material multilayer increases the total thermal resistance for temperatures below 250°C. Increasing the total thermal resistance of the multilayer is a key aspect in the development of PCRAM since having a higher thermal resistance means a more efficient heating of the PCM. A temperature delay in the phase transition wasfound when the number of interfacial thermal resistances is increasing.

However, it was also proven that after the crystallization onset the interfaces between the layers in the GeGST/GST multilayer stack deteriorate. Thus, above 250°C the number of interfaces do not have an influence on the total thermal resistance of the stack in the crystalline phase. This can be explained by a deterioration of the interface quality between layers. Raman analysis showed that after the phase change, the Ge atoms started to migrate in the whole sample, hindering the effect of the doping as consequence.

Moreover, the thermal resistance of the interface between GeGST/GST layers has also been characterized. The value found is in accordance with DMM model and the literature.

ACKNOWLEDGMENTS

This work has received funding from the European Union Horizon 2020 research and innovation program under Grant Agreement No. 824957 (BeforeHand: Boosting Performance of Phase Change Devices by Hetero- and Nanostructure Material Design).

[1] Stanford R Ovshinsky. Reversible electrical switching phenomena in disordered structures. *Physical Review Letters*, 21(20):1450, 1968.

[2] Noboru Yamada, Eiji Ohno, Kenichi Nishiuchi, Nobuo Akahira, and Masatoshi Takao. Rapid-phase transitions of GeTe-Sb2Te3 pseudobinary amorphous thin films for an optical disk memory. *Journal of Applied Physics*, 69(5):2849–2856, 1991.

[3] D Salinga Lencer and MB Grabowski. l. hickel, t. neugebauer, j. and wuttig, m. *Nature Materials*, 7:972–977, 2008.

[4] Simone Raoux, Feng Xiong, Matthias Wuttig, and Eric Pop. Phase change materials and phase change memory. *MRS bulletin*, 39(8):703–710, 2014.

[5] Wei Zhang, Riccardo Mazzarello, Matthias Wuttig, and Evan Ma. Designing crystallization in phase-change materials for universal memory and neuro-inspired computing. *Nature Reviews Materials*, 4(3):150–168, 2019.

[6] Agostino Pirovano, Andrea Leonardo Lacaita, A Benvenuti, F Pellizzer, S Hudgens, and R Bez. Scaling analysis of phase-change memory technology. In *IEEE International Electron Devices Meeting 2003*, pages 29–6. IEEE, 2003.

[7] Roberto Annunziata, P Zuliani, M Borghi, G De Sandre, L Scotti, C Prelini, M Tosi, I Tortorelli, and F Pellizzer. Phase change memory technology for embedded non volatile memory applications for 90nm and beyond. In *2009 IEEE International Electron Devices Meeting (IEDM)*, pages 1–4. IEEE, 2009.

[8] Vivek Seshadri and Onur Mutlu. Simple operations in memory to reduce data movement. In *Advances in Computers*, volume 106, pages 107–166. Elsevier, 2017.

[9] Scott Tyson, Guy Wicker, Tyler Lowrey, Stephen Hudgens, and Ken Hunt. Nonvolatile, high density, high performance phase-change memory. In *2000 IEEE Aerospace Conference. Proceedings (Cat. No. 00TH8484)*, volume 5, pages 385–390. IEEE, 2000.

[10] Fabio Pellizzer, A Pirovano, Federica Ottogalli, M Magistretti, M Scaravaggi, Paola Zuliani, M Tosi, Augusto Benvenuti, P Besana, Sara Cadeo, et al. Novel/spl mu/trench phase-change memory cell for embedded and stand-alone non-volatile memory applications. In *Digest of Technical Papers. 2004 Symposium on VLSI Technology, 2004.*, pages 18–19. IEEE, 2004.

[11] Bin Yu, Xuhui Sun, Sanghyun Ju, David B Janes, and M Meyyappan. Chalcogenide-nanowire-based phase change memory. *IEEE Transactions on Nanotechnology*, 7(4):496–502, 2008.

[12] Massimo Longo, Roberto Fallica, Claudia Wiemer, Olivier Salicio, Marco Fanciulli, Enzo Rotunno, and Laura Lazzarini. Metal organic chemical vapor deposition of phase change Ge1Sb2Te4 nanowires. *Nano letters*, 12(3):1509–1515, 2012.

[13] Feng Xiong, Myung-Ho Bae, Yuan Dai, Albert D Liao, Ashkan Behnam, Enrique A Carrion, Sungduk Hong, Daniele Ielmini, and Eric Pop. Self-aligned nanotube–nanowire phase change memory. *Nano letters*, 13(2):464–469, 2013.

[14] RE Simpson, P Fons, AV Kolobov, T Fukaya, M Krbal, T Yagi, and J Tominaga. Interfacial phase-change memory. *Nature nanotechnology*, 6(8):501–505, 2011.

[15] Ioannis Koltsidas, P Mueller, R Pletka, T Weigold, E Eleftheriou, M Varsamou, A Ntalla, E Bougioukou, A Palli, and T Antonakopoulos. A prototype storage subsystem based on pcm. In *5th Non-Volatile Memories Workshop*, 2014.

[16] Peter Clarke. Intel, micron launch bulk-switching reram. *EE Times*, 2015.

[17] Sungjoo Hong. Memory technology trend and future challenges. In *2010 International Electron Devices Meeting*, pages 12–4. IEEE, 2010.

[18] J Reifenberg, E Pop, A Gibby, S Wong, and K Goodson. Multiphysics modeling and impact of thermal boundary resistance in phase change memory devices. In *Thermal and Thermomechanical Proceedings 10th Intersociety Conference on Phenomena in Electronics Systems, 2006. ITHERM 2006.*, pages 106–113. IEEE, 2006.

[19] Azer Faraclas, Gokhan Bakan, Faruk Dirisaglik, Nicholas E Williams, Ali Gokirmak, Helena Silva, et al. Modeling of thermoelectric effects in phase change mem-

ory cells. *IEEE Transactions on Electron Devices*, 61(2):372–378, 2014.

[20] David L Kencke, Ilya V Karpov, Brian G Johnson, Sean Jong Lee, DerChang Kau, Stephen J Hudgens, John P Reifenberg, Semyon D Savransky, Jingyan Zhang, Martin D Giles, et al. The role of interfaces in damascene phase-change memory. In *2007 IEEE International Electron Devices Meeting*, pages 323–326. IEEE, 2007.

[21] John P Reifenberg, David L Kencke, and Kenneth E Goodson. The impact of thermal boundary resistance in phase-change memory devices. *IEEE Electron Device Letters*, 29(10):1112–1114, 2008.

[22] John P Reifenberg, Kuo-Wei Chang, Matthew A Panzer, Sangbum Kim, Jeremy A Rowlette, Mehdi Asheghi, H-S Philip Wong, and Kenneth E Goodson. Thermal boundary resistance measurements for phase-change memory devices. *IEEE Electron Device Letters*, 31(1):56–58, 2009.

[23] JH Park, S-W Kim, JH Kim, Z Wu, SL Cho, D Ahn, DH Ahn, JM Lee, SU Nam, and D-H Ko. Reduction of RESET current in phase change memory devices by carbon doping in GeSbTe films. *Journal of Applied Physics*, 117(11):115703, 2015.

[24] Q Hubert, C Jahan, V Sousa, L Perniola, A Kusiak, JL Battaglia, P Noé, M Bernard, C Sabbione, M Tessaire, et al. A new insight on IRESET reduction of carbon-doped GST based PCM. In *International Conference on Solid State Devices and Materials (SSDM 2013)*, 2013.

[25] Yunfeng Lai, Baowei Qiao, Jie Feng, Yun Ling, Lianzhang Lai, Yinyin Lin, Tingao Tang, Bingchu Cai, and Bomy Chen. Nitrogen-doped Ge2Sb2Te5 films for nonvolatile memory. *Journal of electronic materials*, 34(2):176–181, 2005.

[26] Minh Anh Luong, Dingfang Wen, Eloise Rahier, Nicolas Ratel Ramond, Béatrice Pécassou, Yannick Le Friec, Daniel Benoit, and Alain Claverie. Impact of nitrogen on the crystallization and microstructure of Ge-rich GeSbTe alloys. *physica status solidi (RRL)–Rapid Research Letters*, 15(3):2000443, 2021.

[27] Liang Tong, Ling Xu, Yifan Jiang, Fei Yang, Lei Geng, Jun Xu, Weining Su, Zhongyuan Ma, and Kunji Chen. Improved phase-change characteristics of Si doped GeSbTe thin films used for phase change memory. *Journal of non-crystalline solids*, 358(17):2402–2404, 2012.

[28] J Feng, Y Zhang, BW Qiao, YF Lai, YY Lin, BC Cai, TA Tang, and B Chen. Si doping in Ge2Sb2Te5 film to reduce the writing current of phase change memory. *Applied Physics A*, 87(1):57–62, 2007.

[29] V Sousa, G Navarro, N Castellani, M Coue, O Cueto, C Sabbione, P Noe, L Perniola, S Blonkowski, P Zuliani, et al. Operation fundamentals in 12Mb phase change memory based on innovative Ge-rich GST materials featuring high reliability performance. In *2015 Symposium on VLSI Technology (VLSI Technology)*, pages T98–T99. IEEE, 2015.

[30] SMS Privitera, I López García, C Bongiorno, V Sousa, MC Cyrille, G Navarro, C Sabbione, E Carria, and E Rimini. Crystallization properties of melt-quenched Ge-rich GeSbTe thin films for phase change memory applications. *Journal of Applied Physics*, 128(15):155105, 2020.

[31] Andrzej Kusiak, Clément Chassain, Alejandro Mateos Canseco, Kanka Ghosh, Marie-Claire Cyrille, Anna Lisa Serra, Gabriele Navarro, Mathieu Bernard, Nguyet-Phuong Tran, and Jean-Luc Battaglia. Temperature-dependent thermal conductivity and interfacial resistance of Ge-Rich Ge2Sb2Te5 films and multilayers. *physica status solidi (RRL)–Rapid Research Letters*, 16(4):2100507, 2022.

[32] Sung-Wook Nam, Cheolkyu Kim, Min-Ho Kwon, Hyo-Sung Lee, Jung-Sub Wi, Dongbok Lee, Tae-Yon Lee, Yoonho Khang, and Ki-Bum Kim. Phase separation behavior of Ge 2 Sb 2 Te 5 line structure during electrical stress biasing. *Applied Physics Letters*, 92(11):111913, 2008.

[33] Marta Agati, Maxime Vallet, Sébastien Joulié, Daniel Benoit, and Alain Claverie. Chemical phase segregation during the crystallization of Ge-rich GeSbTe alloys. *Journal of Materials Chemistry C*, 7(28):8720–8729, 2019.

[34] W Kim, M BrightSky, T Masuda, N Sosa, S Kim, R Bruce, F Carta, G Fraczak, HY Cheng, A Ray, et al. ALD-based confined PCM with a metallic liner toward unlimited endurance. In *2016 IEEE International Electron Devices Meeting (IEDM)*, pages 4–2. IEEE, 2016.

[35] Xilin Zhou, Jitendra K Behera, Shilong Lv, Liangcai Wu, Zhitang Song, and Robert E Simpson. Avalanche atomic switching in strain engineered Sb2Te3–GeTe interfacial phase-change memory cells. *Nano Futures*, 1(2):025003, 2017.

[36] Mattia Boniardi, Jos E Boschker, Jamo Momand, Bart J Kooi, Andrea Redaelli, and Raffaella Calarco. Evidence for thermal-based transition in super-lattice phase change memory (phys. status solidi rrl 4/2019). *physica status solidi (RRL)–Rapid Research Letters*, 13(4):1970021, 2019.

[37] Damien Térébénec, Niccolo Castellani, Nicolas Bernier, Vitomir Sever, Philippe Kowalczyk, Mathieu Bernard, Marie-Claire Cyrille, Nguyet-Phuong Tran, Françoise Hippert, and Pierre Noé. Improvement of phase-change memory performance by means of GeTe/Sb2Te3 superlattices. *physica status solidi (RRL)–Rapid Research Letters*, 15(3):2000538, 2021.

[38] Jean-Luc Battaglia, Andrzej Kusiak, and Kanka Ghosh. The use of photothermal techniques for thermal conductivity and thermal boundary resistance measurements of phase-change chalcogenides alloys. *Journal of Applied Physics*, 129(5):055106, 2021.

[39] Huu Tan Nguyen, Andrzej Kusiak, Jean Luc Battaglia, Cecile Gaborieau, Yanick Anguy, Roberto Fallica, Claudia Wiemer, Alessio Lamperti, and Massimo Longo. Thermal properties of In-Sb-Te thin films for phase change memory application. In *Advances in Science and Technology*, volume 95, pages 113–119. Trans Tech Publ, 2014.

[40] Jean-Luc Battaglia, Andrea Cappella, Enrico Varesi, Vincent Schick, Andrzej Kusiak, Claudia Wiemer, Andrea Gotti, Bruno Hay, et al. Temperature-dependent thermal characterization of Ge2Sb2Te5 and related interfaces by the photothermal radiometry technique. In *Journal of Physics: Conference Series*, volume 214, page 012102. IOP Publishing, 2010.

[41] J-L Battaglia, Andrzej Kusiak, Vincent Schick, Andrea Cappella, Claudia Wiemer, Massimo Longo, and Enrico Varesi. Thermal characterization of the SiO2-Ge2Sb2Te5 interface from room temperature up to 400Â°C. *Journal of Applied Physics*, 107(4):044314, 2010.

[42] G Navarro, V Sousa, P Noé, N Castellani, M Coué, J Kluge, A Kiouseloglou, C Sabbione, A Persico, A Roule, et al. N-doping impact in optimized Ge-rich

materials based phase-change memory. In *2016 IEEE 8th International Memory Workshop (IMW)*, pages 1–4. IEEE, 2016.

[43] Yun Ling, Yinyin Lin, Baowei Qiao, Yunfeng Lai, Jie Feng, Tingao Tang, Bingchu Cai, and Bomy Chen. Effects of si doping on phase transition of ge2sb2te5 films by in situ resistance measurements. *Japanese journal of applied physics*, 45(4L):L349, 2006.

[44] DZ Hu, XM Lu, JS Zhu, and Feng Yan. Study on the crystallization by an electrical resistance measurement in ge 2 sb 2 te 5 and n-doped ge 2 sb 2 te 5 films. *Journal of Applied Physics*, 102(11):113507, 2007.

[45] Tae Hoon Lee, Desmond Loke, and Stephen R Elliott. Microscopic mechanism of doping-induced kinetically constrained crystallization in phase-change materials. *Advanced materials*, 27(37):5477–5483, 2015.

[46] Alain Degiovanni, Christophe Pradere, Emmanuel Ruffio, and Jean-Luc Battaglia. Advanced thermal impedance network for the heat diffusion with sources. *International Journal of Thermal Sciences*, 130:518–524, 2018.

[47] D Maillet and S Andre. J. batsale, a. degiovanni, and c. moyne, thermal quadrupoles, 2000.

[48] DW Mardquardt. An algorithm for least square estimation of parameters. *J. Soc. Ind. Appl. Math*, 11:431–441, 1963.

[49] David D Morrison. Methods for nonlinear least squares problems and convergence proofs. In *JPL SEMINAR PROC. ON TRACKING PROGRAMS AND ORBIT DETERMINATION 26 FEB. 1960*, 1960.

[50] Kenneth Levenberg. A method for the solution of certain non-linear problems in least squares. *Quarterly of applied mathematics*, 2(2):164–168, 1944.

[51] AJ Griffin Jr, FR Brotzen, and PJ Loos. The effective transverse thermal conductivity of amorphous Si3N4 thin films. *Journal of applied physics*, 76(7):4007–4011, 1994.

[52] Eric T Swartz and Robert O Pohl. Thermal boundary resistance. *Reviews of modern physics*, 61(3):605, 1989.

[53] Damien Térébénec, Nicolas Bernier, Niccolo Castellani, Mathieu Bernard, Jean-Baptiste Jager, Martina Tomelleri, Jessy Paterson, Marie-Claire Cyrille, Nguyet-Phuong Tran, Valentina M Giordano, et al. Innovative nanocomposites for low power phase-change memory: GeTe/C Multilayers. *physica status solidi (RRL)–Rapid Research Letters*.

[54] P Němec, Virginie Nazabal, Alain Moréac, J Gutwirth, L Beneš, and M Frumar. Amorphous and crystallized ge–sb–te thin films deposited by pulsed laser: Local structure using raman scattering spectroscopy. *Materials Chemistry and Physics*, 136(2-3):935–941, 2012.

[55] KS Andrikopoulos, SN Yannopoulos, GA Voyiatzis, AV Kolobov, Michel Ribes, and J Tominaga. Raman scattering study of the a-gete structure and possible mechanism for the amorphous to crystal transition. *Journal of physics: condensed matter*, 18(3):965, 2006.

[56] Eloïse Rahier, Sijia Ran, Nicolas Ratel Ramond, Shuangying Ma, Lionel Calmels, Sabyasachi Saha, Cristian Mocuta, Daniel Benoit, Yannick Le Friec, Minh Anh Luong, et al. Crystallization of ge-rich gesbte alloys: The riddle is solved. *ACS Applied Electronic Materials*, 2022.

[57] Lucie Prazakova, Emmanuel Nolot, Eugénie Martinez, Frederic Fillot, Denis Rouchon, Névine Rochat, Mathieu Bernard, Chiara Sabbione, Damien Morel, Nicolas Bernier, et al. Temperature driven structural evolution of ge-rich gesbte alloys and role of n-doping. *Journal of Applied Physics*, 128(21):215102, 2020.

[58] L Prazakova, E Nolot, E Martinez, D Rouchon, F Fillot, N Bernier, R Elizalde, M Bernard, and G Navarro. The effect of ge content on structural evolution of ge-rich gesbte alloys at increasing temperature. *Materialia*, 21:101345, 2022.

[59] Clément Chassain, Andrzej Kusiak, Kevin Krause, Marine Garcia, and Jean-Luc Battaglia. Bayesian estimation of thermal properties using periodically pulsed photothermal radiometry: A focus on interfacial thermal resistances between layers. *physica status solidi (RRL)–Rapid Research Letters*, page 2200328, 2022.

[60] Kiumars Aryana, John T Gaskins, Joyeeta Nag, Derek A Stewart, Zhaoqiang Bai, Saikat Mukhopadhyay, John C Read, David H Olson, Eric R Hoglund, James M Howe, et al. Interface controlled thermal resistances of ultrathin chalcogenide-based phase change memory devices. *Nature communications*, 12(1):1–11, 2021.

[61] Jean-Luc Battaglia, Andrzej Kusiak, Abdelhak Saci, Roberto Fallica, Alessio Lamperti, and Claudia Wiemer. Effect of a thin Ti interfacial layer on the thermal resistance of Ge2Sb2Te5-TiN stack. *Applied Physics Letters*, 105(12):121903, 2014.